Chemical Engineering Journal 374 (2019) 832–839

Contents lists available at ScienceDirect

Chemical Engineering Journal

journal homepage: www.elsevier.com/locate/cej

The self-protection effect of reactant gas on the moisture stability of CuSAPO-34 catalyst for NH_3-SCR

Yi Cao[a], Dong Fan[a], Lijng Sun[a,b], Miao Yang[a], Lei Cao[a], Tantan Sun[a,b], Shutao Xu[a], Peng Tian[a,*], Zhongmin Liu[a,*]

[a] National Engineering Laboratory for Methanol to Olefins, Dalian National Laboratory for Clean Energy, Dalian Institute of Chemical Physics, Chinese Academy of Sciences, Dalian 116023, PR China
[b] University of Chinese Academy of Sciences, Beijing 100049, PR China

HIGHLIGHTS

- The moisture stability of CuSAPO-34 is improved by NH_3-SCR reactant gas.
- The adspecies on CuSAPO-34 after NH_3-SCR reaction are NH_3 species.
- NH_3 adspecies prevent the decay of Brönsted acid sites and reducibility of Cu^{2+}.
- The protection effect of NH_3 adspecies is prominent when T ≤ 300 °C.
- The stability of CuSAPO-34 can be improved by adjusting its location in tailpipe.

GRAPHICAL ABSTRACT

The low-temperature moisture stability of CuSAPO-34 catalyst is improved by NH_3-SCR reactant gas which exists in working condition.

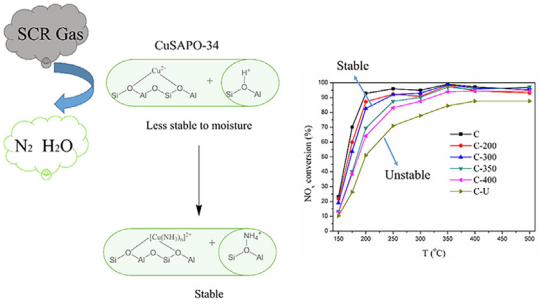

ARTICLE INFO

Keywords:
CuSAPO-34
Stability
Residual adspecies
Self-protection
NH_3-SCR

ABSTRACT

The surface of CuSAPO-34 catalysts after NH_3-SCR reaction (T ≤ 400 °C) is revealed to have residual adspecies. Cycle hydration methods are designed to explore the influence of the residual species upon the moisture stability of CuSAPO-34. It is demonstrated that the residual species on the catalyst surface are NH_3 adspecies, which could help inhibit the transformation of $Si(OAl)_4$ species to Si islands and prevent the decay of Brönsted acid sites (BAS) during the hydration treatment; the better preserved acidity and the existence of NH_3 facilitate the preservation of isolated Cu^{2+} ions and their reducibility, and thus the SCR activity of the catalysts. The protective effect of residual NH_3 species against the low-temperature water vapor is prominent when T ≤ 300 °C, which declines gradually and becomes weak when T > 400 °C due to the desorption of NH_3 adspecies. The present work implies that the moisture stability of CuSAPO-34 catalyst could be simply ameliorated by locating it in an appropriate zone of the tailpipe to avoid the excessive desorption of the NH_3 adspecies.

1. Introduction

NO_x emitted from lean burn vehicles is a major atmospheric pollutant, which causes serious environmental issues [1,2]. NH_3-SCR technology has been regarded as one of the most efficient technologies to eliminate NO_x, in which NH_3 is supplied by the *in situ* hydrolysis of urea [3]. The typical after-treatment system consists of diesel oxidation catalyst (DOC), diesel particulate filter (DPF), SCR catalyst and

* Corresponding authors.
E-mail addresses: tianpeng@dicp.ac.cn (P. Tian), liuzm@dicp.ac.cn (Z. Liu).

https://doi.org/10.1016/j.cej.2019.05.227
Received 8 April 2019; Received in revised form 30 May 2019; Accepted 31 May 2019
Available online 01 June 2019
1385-8947/

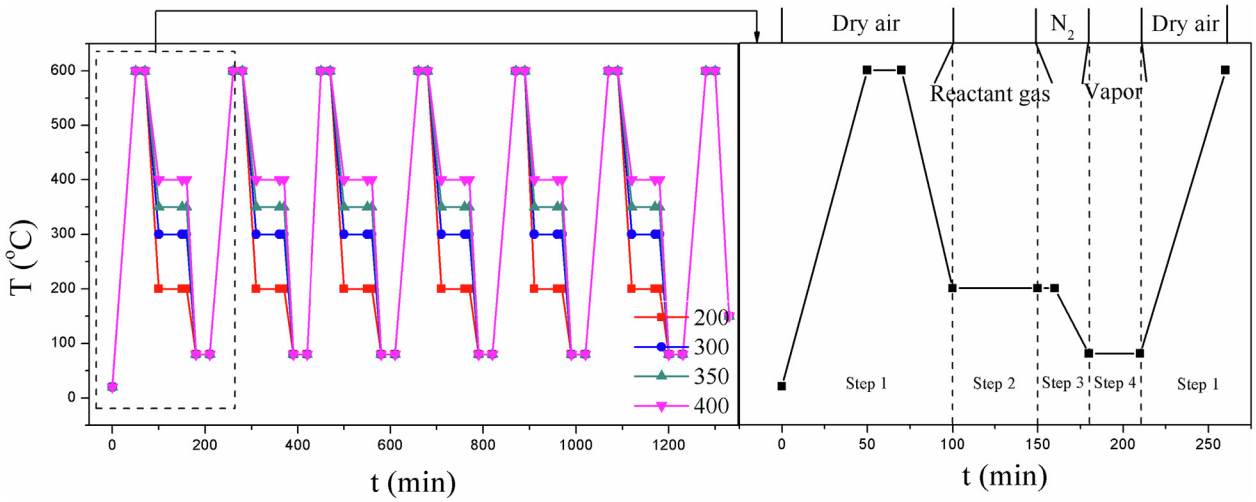

Fig. 1. The detailed treatment procedures for CuSAPO-34 catalysts. The procedures are designed to investigate the effect of the residual surface adspecies after the NH_3-SCR reaction on the moisture stability of CuSAPO-34. Four contact temperatures of NH_3-SCR feed gas with the catalyst are investigated (200–400 °C). The subsequent hydration temperature is 80 °C. The procedure is repeated for 6 times.

ammonia slip catalyst (ASC) in sequential [2]. In practice, periodical regeneration is needed for the DPF, and a great deal of heat will immediately transfer to the SCR unit (> 700 °C) [4]. Thus, excellent hydrothermal stability is a basic requirement for SCR catalysts. In recent years, CuSAPO-34 catalyst receives much attention due to its excellent NH_3-SCR performance, high N_2 selectivity, outstanding hydrocarbon resistance and high temperature hydrothermal stability [5–8].

One drawback that limits the practical application of CuSAPO-34 is its high sensitivity to the low temperature vapor [9,10], since the SCR catalyst has to encounter humid air during the cold-start or turn-off period of the diesel engine. Leistner et al. once reported that the low-temperature activity of CuSAPO-34 catalyst dropped sharply after hydration treatment at 70 °C for 12 h. They claimed that the deactivation of CuSAPO-34 was caused by the decrease of active Cu species upon hydration treatment [11]. Wang et al. investigated the hydration stability of CuSAPO-34 with different Cu contents and found that the sample with low content of Cu suffered an obvious activity drop upon hydration treatment, similar as the results of Leistner. However, the deterioration of CuSAPO-34 catalyst was ascribed to the framework collapse, the decline of acid sites and the loss of active sites [12]. In addition, we recently investigated the effect of hydration methods on the stability of CuSAPO-34. It was revealed that compared with simply prolonging the hydration duration, cycle hydration treatment with repeated hydration-calcination processes, which is closer to the conditions of practical use of the catalyst, could induce a faster loss of the strong BAS and a more pronounced decline of the reducibility of cupric ions [13].

In practical application, except for the time during DPF regeneration, the inlet temperature of the SCR unit is generally lower than 400 °C [3,14]. The NH_3 used for the SCR reaction is supplied by the hydrolysis of urea. The urea dosing system starts to work above 180 °C, at which temperature the complete hydrolysis of urea occurs [3,15]. Therefore, the main operation temperature range of SCR catalyst is between 180 and 400 °C. In addition, the surface of the CuSAPO-34 SCR catalyst under working conditions should be unclean, which might be covered by NH_3 species or NO_x species. After the turn-off of the NH_3-SCR system, these adspecies will reside (partially or completely) on the surface of the catalyst, and exert influence on the stability of the catalyst. However, as far as we know, less attention has been drawn to the effect of these residual adspecies on the performance of CuSAPO-34 catalyst.

Herein, we investigated the residual adspecies on the surface of CuSAPO-34 catalyst after NH_3-SCR reaction, as well as the effect of residual adspecies on the moisture stability of CuSAPO-34. Interestingly, it is demonstrated that the residual adspecies have a powerful protection effect on the stability of CuSAPO-34 toward low-temperature moisture.

2. Experimental

2.1. Synthesis, ion exchange and low-temperature hydration conditions

SAPO-34 was synthesized using diethylamine (DEA) as a template. The gel molar ratio was $2.0DEA/0.4SiO_2/1.0Al_2O_3/1.0P_2O_5/50H_2O$. The detailed synthetic procedure can be found in our recent study [13].

Direct-ion-exchange method was used to prepare CuSAPO-34 catalyst [16]. 5 g as-made molecular sieve was mixed with 100 g Cu $(CH_3COO)_2$ solution (0.01 mol/L) at 50 °C. After stirring for 5 h, the solid was separated, washed and dried at 110 °C. The as-made sample was calcined in air at 600 °C for 5 h to remove the organics. The Cu content and molar composition of SAPO-34 was 1.14 wt% and $Si_{0.122}Al_{0.495}P_{0.383}O_2$ (XRF), respectively. The obtained fresh sample was named as C.

The moisture stability of the catalyst was investigated by cycle hydration procedure developed by us recently [13]. The calcined catalyst was first hydrated at 80 °C under 10% H_2O/N_2 flow (253.4 mL/min) for 30 min. Afterwards, the catalyst was heated to 600 °C in dry airflow immediately. The hydration treatment was repeated for 6 times. More details about the hydration process can be found in our previous study [13]. The final sample was denoted as C-U.

To investigate the influence of the residual surface adspecies after the NH_3-SCR reaction on the moisture stability of CuSAPO-34 catalyst, feed gas (322 mL/min) containing NH_3 (500 ppm), NO (500 ppm), O_2 (6.4%), H_2O (6.4%) and N_2 flowed through the calcined catalyst at desired temperature for 50 min. Then, the catalyst was treated by dry N_2 for 10 min, and cooled to 80 °C in N_2 (150 mL/min). Subsequently, hydration treatment was conducted at 80 °C under a flow of 10% H_2O in N_2 flow (253 mL/min) for 30 min. After that, the treated catalyst was heated to 600 °C in a flow of dry air. The procedure was repeated for 6 times. The final sample was labeled as C-X (X represents the contact temperature of NH_3-SCR feed gas with the catalyst). Detailed treatment procedures are illustrated in Fig. 1.

In addition, similar treatment procedures as those of the C-X catalysts except using NO oxidation gas (NH_3-SCR feed gas without NH_3) or NH_3 oxidation gas (NH_3-SCR feed gas without NO) were conducted to distinguish the effect of each reagent. The final samples were denoted

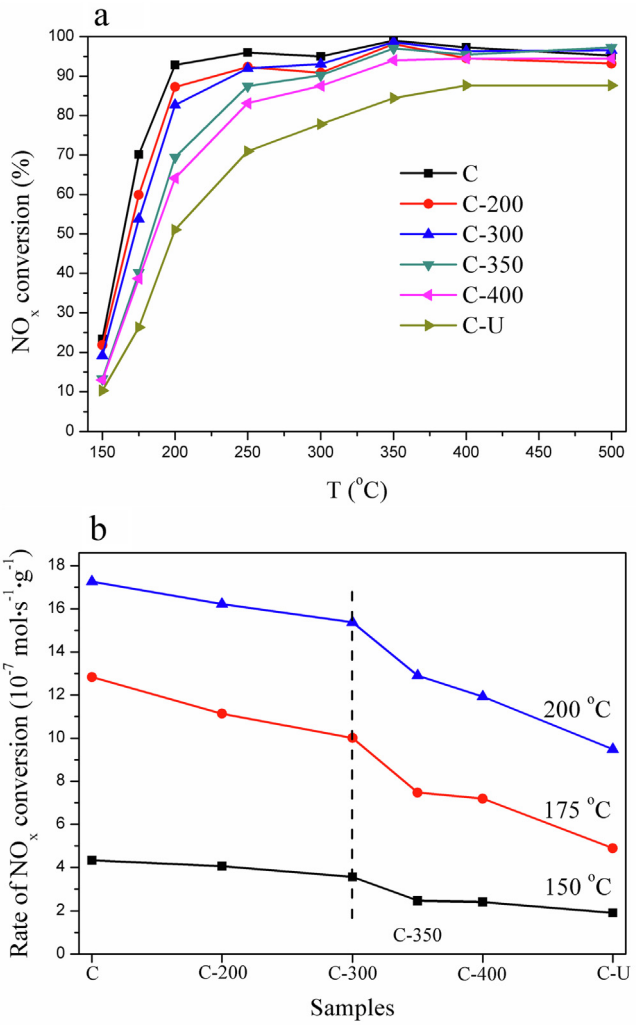

Fig. 2. (a) Conversion of NO_x on CuSAPO-34 catalysts before and after hydration treatment, NH_3-SCR feed gas was used for the treatment of catalysts C-X. (b) Comparison of NO_x conversion rate of the catalysts at 150, 175 and 200 °C.

as C-X-NH_3 (using NH_3 oxidation gas) and C-X-NO (using NO oxidation gas), where X represents the contact temperature of feed gas with the catalyst.

2.2. Catalyst tests

NH_3-SCR reaction was carried out in a fixed-bed quartz reactor as our previous study [13]. For each test, 0.060 g of CuSAPO-34 and 0.240 g of quartz beads (60–80 mesh) were blended and put into the reactor. The catalyst was activated in N_2 at 550 °C for 2 h prior to activity test. The feed gas contained NO (500 ppm), NH_3 (500 ppm), H_2O (6.4%), O_2 (6.4%) and N_2. The gas hourly space velocity (GHSV) was controlled as 300,000 h^{-1} (0.32 L/min of total feed rate). The gas compositions (NO, NO_2 and N_2O) were continually monitored by an FTIR spectrometer (Bruker). The FTIR spectra were collected after the reaction reaching a steady state (about 40 min).

The formula shown below were used to determine the NO_x conversion and reaction rate:

$$NO_x \text{ conversion } (\%) = \frac{([NO]_{in} - [NO]_{out} - [NO_2]_{out} - 2[N_2O]_{out})}{[NO]_{in}} \times 100\ \% \quad (1)$$

$$\text{rate} = \frac{NO_x \text{ conversion } (\%) \times F \times [C]}{22.4 \times m} (\text{mol}\cdot\text{g}^{-1}\cdot\text{s}^{-1}) \quad (2)$$

Herein, F is 0.32 L/min (feed rate), [C] is 500 ppm (inlet NO_x concentration) and m is 0.06 g (catalyst weight).

2.3. Catalyst characterization

In situ DRIFTS spectra were collected using a FTIR spectrometer (Bruker) with high temperature chamber (ZnSe windows) and MCT detector (64 scans, 4 cm^{-1} resolution). Before measurements, the sample was activated in N_2 (40 mL/min) at 500 °C for 40 min. Background spectrum of the sample associated to each temperature was recorded in N_2 flow independently. For NH_3-TPD measurements, the sample was first exposed to 1000 ppm of NH_3 at 150 °C for 40 min. After purging with N_2 to reach a steady spectrum, the sample was heated to specific temperature in N_2 (20 mL/min). The spectrum was collected after purging for 40 min at each specific temperature. NH_3-SCR surface reaction was conducted at 150, 200, 300, 350 and 400 °C, respectively. A feed gas (40 mL/min) containing 500 ppm NO, 500 ppm NH_3, 6.4% of O_2 and N_2 for balance passed through the sample for 40 min. Then the spectrum was collected after purging the catalyst by N_2 for 40 min (20 mL/min) at each specific temperature.

N_2 adsorption isotherms of the samples were determined on a Micromeritics ASAP 2020 at −196 °C. Before analysis, each sample was outgassed at 350 °C for 360 min. The micropore areas and volumes were evaluated by t-plot method. The relative micropore areas were calculated by the following formula:

$$R_s = \frac{micropore\ \ area\ of\ the\ \ sample}{micropore\ area\ of\ the\ \ sample\ \ C} \times 100\% \quad (3)$$

The elemental composition was detected on a PANalytical X-ray fluorescence (XRF) spectrometer. The ^{29}Si MAS NMR spectra were measured using Bruker Avance III 600 spectrometer operating at 14.1 T using a 4 mm double resonance MAS probe. The resonance frequency of ^{29}Si was 119.2 MHz. The spinning rates were 8 KHz using high power proton decoupling. 4096 scans were accumulated with a π/4 pulse width of 2 μs and a 10 s recycle delay. Kaolinite was utilized to calibrate the chemical shifts. The powder XRD patterns were recorded on a PANalytical X'Pert Pro X-ray diffractometer (Cu kα radiation). The relative crystallinity of the samples was calculated from the three strongest peaks in the XRD patterns. H_2-TPR and NH_3-TPD measurements were performed on a Micromeritics AutoChem II analyzer. For H_2-TPR, the sample (80 mg) was first degassed at 500 °C for 60 min under Ar (30 mL/min) and then cooled to 100 °C. H_2-TPR was performed from 100 to 700 °C in 10% H_2/Ar flow (10 °C/min, 30 mL/min). For NH_3-TPD, the sample (100 mg) was degassed at 500 °C for 60 min under He and then cooled down to 120 °C. After that the sample was saturated with NH_3 under a flow of 2% NH_3/He (30 mL/min) and further flushed with He (30 mL/min) until the baseline was steady. Subsequently, NH_3 desorption was carried out in the range of 120–600 °C at a rate of 10 °C/min in flowing He (30 mL/min). The EPR spectra of Cu^{2+} ions were measured on Bruker A200 X-band spectrometer at −170 °C (9.50 GHz, 1.998 mW). The sweep field was in the range of 2000–4000 Gauss (G). The amount of cupric ions over the sample was quantified by standard cupric sulfate solution. The dehydrated samples for the test were prepared as our previous study [13].

3. Results and discussion

3.1. Catalytic performance

Fig. 2a displays the NO_x conversion results of the CuSAPO-34 before and after different hydration treatments. The best catalytic performance is observed for the fresh catalyst (sample C). The catalyst C-U, which was obtained simply by low-temperature cycle hydration treatment,

shows the worst catalytic activity. For the C-X catalyst series prepared by repeated contacts of NH_3-SCR feed gas (step 2 in Fig. 1) and low-temperature hydration treatments (step 4 in Fig. 1), higher reaction activities were observed, indicating an enhanced moisture stability. Given the different treatment procedures for C-U and C-X catalysts, it is speculated that some adspecies form and reside on the catalyst surface during the feed gas contact treatment (step 2 in Fig. 1) and might provide certain protection effect and thus help improve the moisture stability of catalysts C-X. Besides, with the rise of the contact temperature, the NH_3-SCR activities, more prominently for those located in the low-temperature range, show a declining trend for the C-X catalyst series. This implies that the lower the *in situ* feed gas contact temperature is, the better the protection effect we could get. To better compare the activity change with the variation of the contact temperature of NH_3-SCR feed gas, the NO_x conversion rates derived from Fig. 2a at low temperatures are plotted and given in Fig. 2b. Clearly, the protection effect of NH_3-SCR gas on CuSAPO-34 is strong when the contact temperature is ≤ 300 °C; further increasing the contact temperature to 350 and 400 °C, the protection effect decreases drastically. The N_2 selectivity on CuSAPO-34 catalysts is displayed in Fig. A1, which is very high (> 96%) even after low-temperature hydration treatment.

To identify the exact component associated with the protection effect in the NH_3-SCR feed gas, NH_3-free feed gas (NO oxidation gas) was used for the catalyst treatment procedures as illustrated in Fig. 1. The corresponding reaction results are displayed in Fig. A.2. Compared with the fresh catalysts, an obvious activity decrease could be observed for the hydrated catalyst treated with NO oxidation gas, suggesting the trivial protection effect of NO oxidation gas. Moreover, the effect of NO-free feed gas (NH_3 oxidation gas) was also explored. From Fig. 3a, all the hydrated catalysts treated with NH_3 oxidation gas possess higher NH_3-SCR activities than the catalyst C-U, indicating that NH_3 oxidation gas treatment is beneficial for the moisture stability of CuSAPO-34 catalyst. To better indicate the activity variation as the contact temperature of NH_3 oxidation gas, the NO_x conversion rates of the catalysts at 150, 175 and 200 °C are plotted and given in Fig. 3b. Obviously, the protection effect of NH_3 oxidation gas upon the moisture stability of CuSAPO-34 resembles that of NH_3-SCR feed gas (Fig. 2b). The above results indicate that the NH_3 in NH_3-SCR feed gas is crucial for improving the moisture stability of CuSAPO-34.

3.2. NH_3 adspecies on CuSAPO-34 catalyst

NH_3-TPD experiments were conducted to monitor the amount of NH_3 adsorption on the fresh CuSAPO-34 at different temperatures. The profiles are displayed in Fig. 4. When the adsorption temperature of NH_3 is at 120 °C, two obvious desorption peaks centered at 194 and 429 °C can be observed, which correspond to weak and moderate/strong acid sites, respectively. With the elevation of NH_3 adsorption temperature to 200 °C, one desorption peak centered at 429 °C together with a shoulder around 300 °C are present. Further increasing the NH_3 adsorption temperature to 300 and 350 °C, only symmetrical desorption peaks centered around 429 °C could be recorded, the area of which drops with the rising of adsorption temperature. For the sample that adsorbs NH_3 at 400 °C, its NH_3-TPD profile only contains a very small peak at 504 °C, resulting from NH_3 desorption from stronger acid sites. By assuming that the coverage of NH_3 on CuSAPO-34 at 120 °C is 100%, the relationship between the NH_3 coverage and temperature is plotted and shown in Fig. 4 (inset). Clearly, the NH_3 coverage reduces linearly with the increase of NH_3 adsorption temperature.

In-situ DRIFTS was further used to probe the NH_3 adspecies over the fresh CuSAPO-34 catalyst. The fresh catalyst was first saturated with NH_3 under a NH_3(500 ppm)-N_2 flow at 150 °C for 40 min and then flushed with N_2 until the spectrum was stable. As displayed in Fig. 5, the negative bands at 900 and 850 cm^{-1} are ascribed to the perturbation of T-O-T bonds by exchanged copper ions, which are consumed

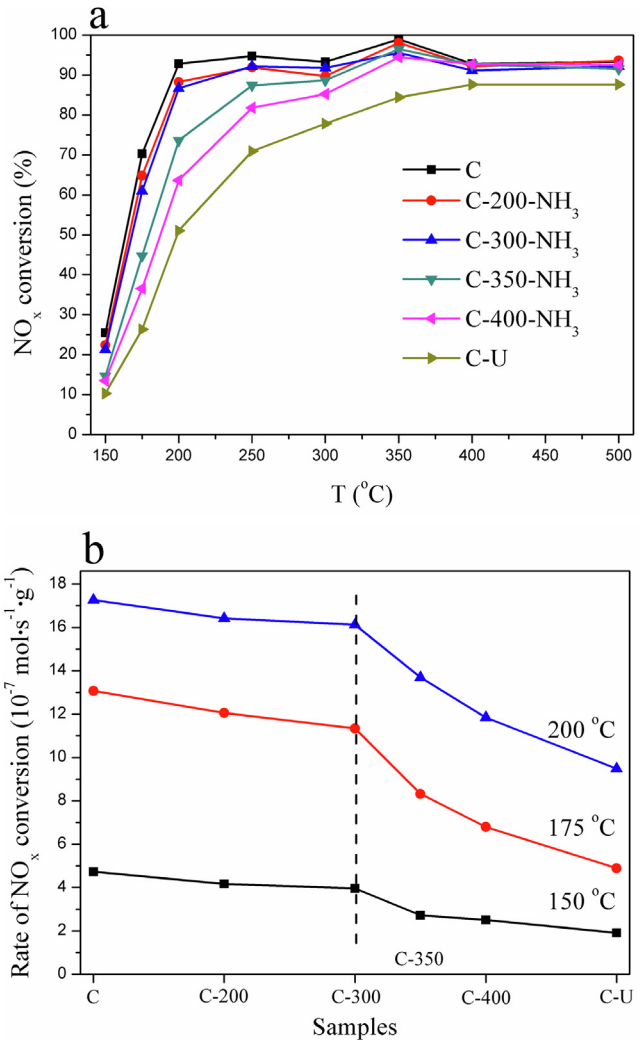

Fig. 3. (a) Conversion of NO_x on CuSAPO-34 catalysts before and after hydration treatment, NH_3 oxidation gas (NH_3-SCR feed gas without NO) was used for the treatment of catalysts C-X-NH_3. (b) Comparison of NO_x conversion rate of the catalysts at 150, 175 and 200 °C.

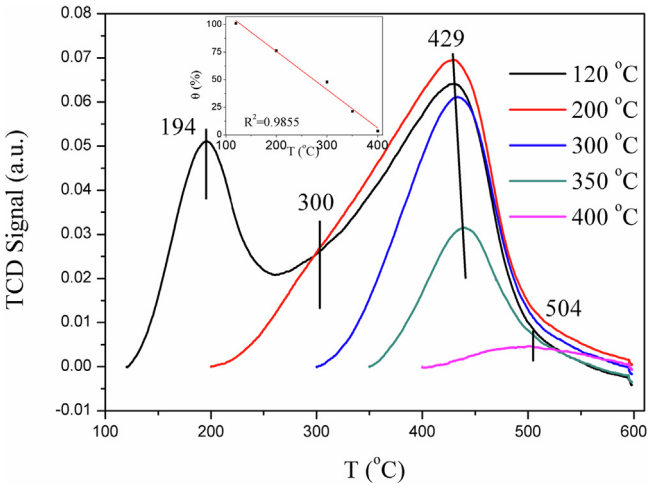

Fig. 4. NH_3-TPD curves of the fresh CuSAPO-34 samples that adsorbed NH_3 at different temperatures. The insert shows the relationship between the NH_3 coverage and the NH_3 adsorption temperature.

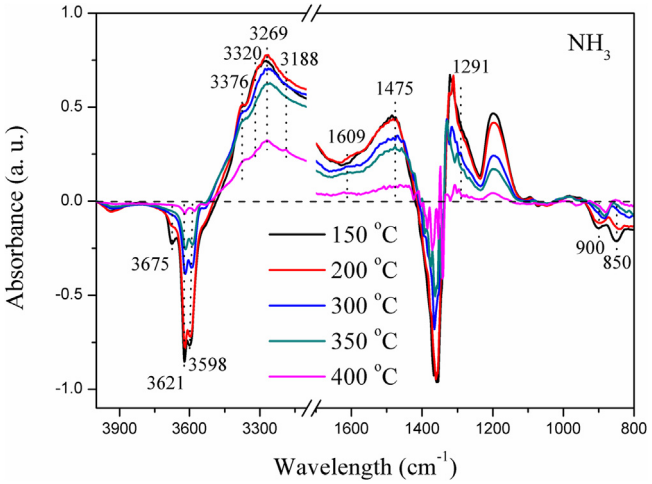

Fig. 5. NH_3-TPD DRIFT spectra of the fresh CuSAPO-34 samples. Each spectrum was collected after N_2 purging at each specific temperature for 40 min.

upon NH_3 adsorption due to the weakened interaction between the copper ions and the zeolite framework [17,18]. The bands at 1609/1291 and 1475 cm^{-1} arise from the N–H bending vibration of NH_3 adsorbed on the Lewis acid sites (LAS) and BAS, respectively [19,20]. The N–H stretching vibration region is located in the range of 3000 to 3400 cm^{-1}, in which the positive bands at 3376, 3320, 3289 and 3188 cm^{-1} are attributed to the physisorbed NH_3 molecule, the symmetric vibration of NH_4^+, the asymmetric vibration of NH_4^+ and the NH_3 adsorbed on the Cu ions [19,21], respectively. In addition, the negative band at 3675 cm^{-1} is due to the consumption of P-OH bond by NH_3 [19,21], and the negative bands at 3621 and 3598 cm^{-1} are correlated with the consumption of Si-OH-Al bonds located at 8R channel and D6R [22,23], respectively.

To study the desorption behavior of NH_3 adspecies, NH_3-TPD DRIFT was performed and the collected spectra are displayed in Fig. 5. When the desorption temperature increases from 150 to 200 °C, the negative band at 3675 cm^{-1} ascribed to NH_3 on P-OH reduces drastically, while the bands at 3621 and 3598 cm^{-1} corresponding to the Si–OH–Al bonds only present a slight decrease, indicating that the desorption peak at 195 °C in Fig. 4 mainly originates from the NH_3 desorption from P-OH and a slight amount of weak BAS. Further elevating the desorption temperature, the bands at 3621 and 3598 cm^{-1} reduce significantly, and the corresponding exposure of the Si–OH–Al bonds is calculated to be 50% at 300 °C and 90% at 400 °C according to the recovery percentage of the peak area. The simultaneous decrease of the bands at 3621 and 3598 cm^{-1} implies that the BAS located in the 8R channel and D6R have similar acid strength. Meanwhile, with the rise of the desorption temperature above 200 °C, a drop trend could also be observed for the bands at 1475 and 1609 cm^{-1}. It implies that the desorption peak at 429 °C in Fig. 4 contains the contribution of NH_3 desorbed from both LAS and BAS. Notably, after desorption at 400 °C, weak absorbance signals at 1475 and 1609 cm^{-1} could still be discerned, corresponding to the residual NH_3 adsorption on the BAS and LAS with relatively stronger acidities. This is congruent with the presence of the tiny desorption peak at 504 °C in Fig. 4.

3.3. The residual surface adspecies on the CuSAPO-34 catalyst after the NH_3-SCR process

In-situ DRIFTS was employed to investigate the surface adspecies on the CuSAPO-34 after the SCR reaction at different temperatures. The spectra are presented in Fig. 6. The shapes and positions of the bands in Fig. 6a are quite similar to those in Fig. 5, implying the existence of adsorbed NH_3 on the catalyst surface. A mixture of NO and O_2 gas was introduced to probe the NO_x adspecies on CuSAPO-34 (Fig. A.3). As

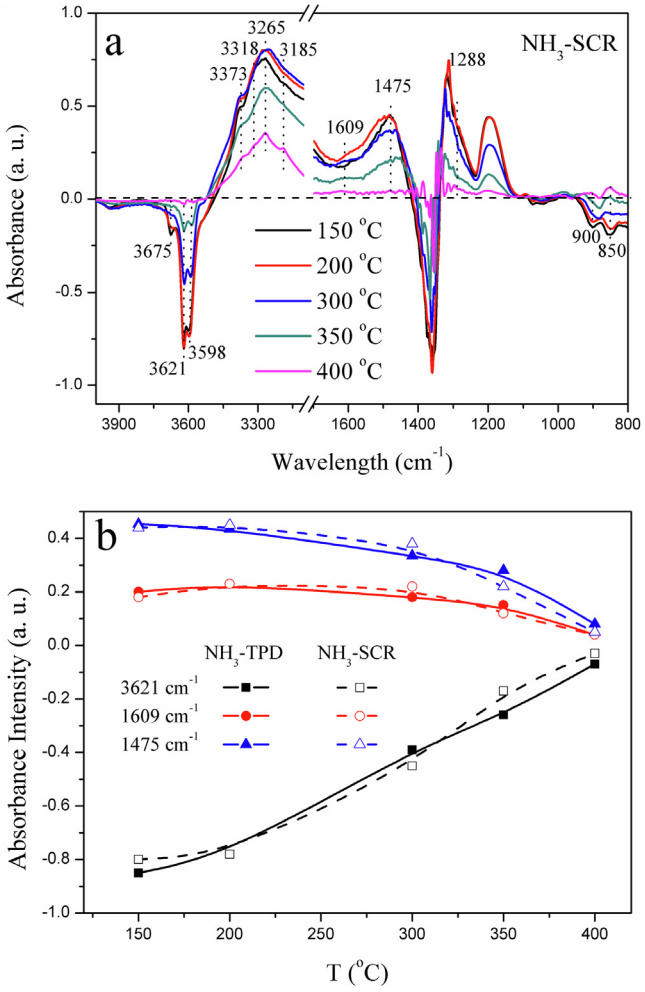

Fig. 6. (a) *In-situ* DRIFTS spectra of the fresh CuSAPO-34 after the NH_3-SCR process at different temperatures. Each spectrum was collected after exposing the catalyst in the NH_3-SCR gases for 40 min followed by N_2 purging for 40 min at specific temperature. (b) Intensity comparison of NH_3 adspecies-related signals during the NH_3-SCR and NH_3-TPD processes.

displayed in Fig. A.3, upon the adsorption of NO_x species, an increase of the positive bands at 900 and 850 cm^{-1} could be observed, indicating an enhanced interaction between the copper ions and the framework, which should result from the adsorption of NO_x on Cu ions. Since no positive bands at 900 and 850 cm^{-1} can be observed in Fig. 6a, the adsorbability of NO_x adspecies on the catalyst is supposed to be much weaker than that of NH_3 during the SCR reaction. TPD-MS experiments were also conducted to detect the residual species over the surface of CuSAPO-34 after NH_3-SCR reaction. From Fig. A.4, it is clear that certain amounts of NH_3 are retained on the catalyst after SCR reaction at 200 °C, which become rare after reaction at higher temperature of 400 °C. However, no signals due to the NO_x adspecies can be discerned over the catalyst surface, irrespective of the reaction temperature.

Fig. 6b further compares the intensity of NH_3 adspecies-related signals on CuSAPO-34 during the NH_3-SCR process and NH_3-TPD process. It is clear that both the intensity and variation trend following the temperature change are similar for the two sets of DRIFTS experiments, confirming that the residual surface adspecies on CuSAPO-34 catalyst after the NH_3-SCR process are NH_3 species.

Table 1
The textural properties and relative crystallinity of the CuSAPO-34 catalysts before and after hydration treatments.

Sample	S_{micro}[1] (m^2/g)	V_{micro}[2] (cm^3/g)	R_s (%)[3]	R_x (%)[4]
C	683	0.27	100	100
C-200	647	0.27	94.7	94
C-300	622	0.26	91.1	98
C-350	644	0.27	94.3	95
C-400	670	0.28	98.1	90
C-U	681	0.28	99.7	89

[1]Micropore surface area. [2]Micropore volume. [3]Relative micropore surface area. [4]Relative crystallinity (XRD results are shown in Fig. A.5).

3.4. The physicochemical properties of the CuSAPO-34 catalysts after different hydration treatment procedures

3.4.1. Texture and structure

Table 1 presents the textural properties and relative crystallinity of the samples. Both the relative microporous surface area (R_s) and the relative crystallinity (R_x) of the treated samples are maintained at high levels, indicating that different low-temperature hydration treatment procedures in the present study have little impact on the texture and structure of CuSAPO-34 samples.

3.4.2. Acid properties

It is well known that the acidity of the CuSAPO-34 catalysts is essential for their SCR performance. Wang et al. reported that CuSAPO-34 with larger amounts of strong BAS had better SCR performance [19]. Recently, we confirmed that the decline of strong acid sites would cause the decay of NH_3-SCR performance [13]. In this study, NH_3-TPD was employed to monitor the protection effect of surface NH_3 adspecies on the acid sites of CuSAPO-34 against the hydration treatment. From Fig. 7a, it is evident that the acid concentrations of the catalysts C-X prepared by repeated contacts of NH_3-SCR feed gas and hydration treatments are larger than that of the catalyst C-U, indicating that the residual NH_3 adspecies on the former catalysts can help preserve the acid sites during the hydration treatment process.

Fig. 7b shows the de-convoluted results of the NH_3-TPD curves of the samples. Similar amounts of the weak acid sites are observed on all the investigated catalysts, suggesting that the those sites are barely perturbed by treatment procedures. The strong acid sites are also well maintained when the contact temperature is below 300 °C (samples C-200 and C-300). However, further increasing the contact temperature to 350 °C (sample C-350) and 400 °C (sample C-400), the amounts of the strong acid sites gradually decline. Since the content of the LAS over the samples is relatively low, the reduction of the strong acid sites should be mainly owing to the deterioration of the BAS. The deterioration trend in strong acid sites consists with the decline of NO_x conversion of the catalysts.

Note that a turning point could be observed in the variation curve of the strong acid sites (Fig. 7b, sample C-300). Given that the exposed Brönsted acid sites without NH_3 perturbation rise pseudo-linearly with the increase of NH_3-SCR reaction temperature as evidenced by *in-situ* DRIFTS (Fig. 6b), the presence of the turning point in Fig. 7b suggests that a critical value of surface NH_3 content exists for the better preservation of the strong acid sites. More specifically, the residual NH_3 adspecies on the catalyst surface treated at T ≤ 300 °C could provide better protection for the acidic Si-OH-Al bonds against hydrolysis (the amount of NH_3 adspecies > critical value); at higher treatment temperatures, the amount of the residual NH_3 adspecies drops, which leads to the degradation of the protection effect and hence a prominent decline of the strong acid sites.

3.4.3. ^{29}Si MAS NMR

The BAS of SAPO-34 are correlated to the Si species in the SAPO-34 framework [24]. Hence, ^{29}Si MAS NMR was conducted to probe the Si species in the CuSAPO-34 catalysts. From Fig. 8 and Fig. A.6, the ^{29}Si spectrum of the fresh catalyst C presents one strong peak at −95 ppm ascribed to $Si(OAl)_4$ species, and one tiny shoulder resonance at around −101 ppm due to $Si(OAl)_3$ species [9,25], indicating that the majority of the BAS in sample C are derived from $Si(OAl)_4$ species.

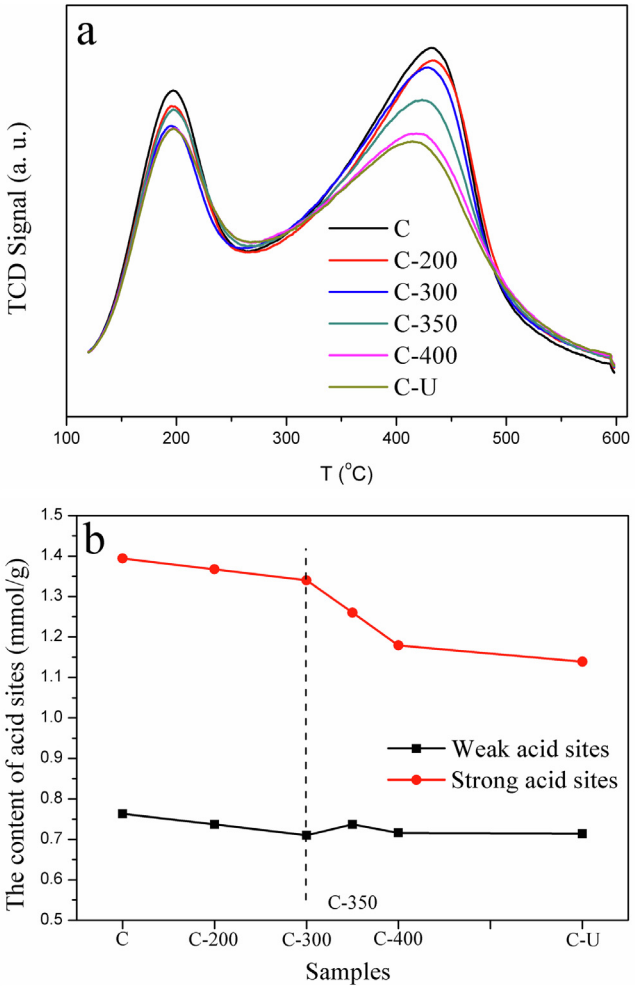

Fig. 7. (a) NH_3-TPD curves of the CuSAPO-34 samples, (b) The variation of weak and strong acid sites over the catalysts.

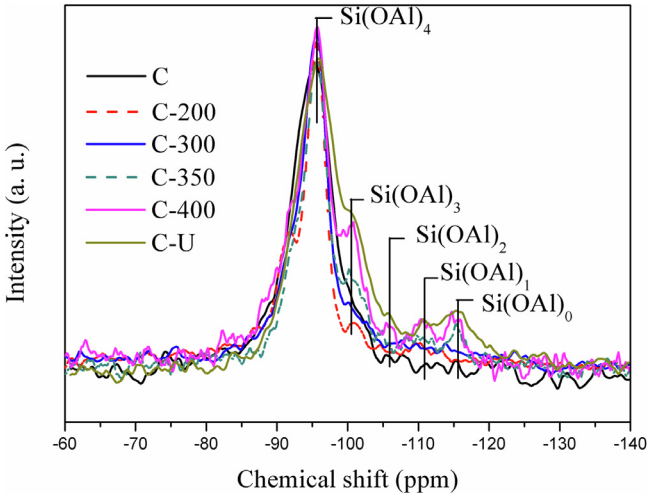

Fig. 8. ^{29}Si MAS NMR spectra of the CuSAPO-34 catalysts.

After hydration treatments, resonances due to $Si(OAl)_2$, $Si(OAl)_1$ and $Si(OAl)_0$ species arise at −105.9, −110.6 and −115.6 ppm, respectively. Note that no signals due to the defect Si, Al and P species (Figs. A.6 and A.7) could be discerned, indicating that part of the Si $(OAl)_4$ species are directly transformed to Si islands without damage to the structural integrity. This phenomenon is consistent with our previous results [13].

Fig. A.6 displays the de-convoluted ^{29}Si MAS NMR spectra. The quantitative results are summarized in Table A.1. It can be found that the Si environments over samples C-200 and C-300 are similar to those of the fresh sample. With the rising of the contact temperature (the hydrated catalysts C-350 and C-400), the ratio of Si islands apparently increases, in accordance with the transformation of $Si(OAl)_4$ species and the reduction trend of the strong acid sites. The formation of Si-islands should be caused by the migration and aggregation of the adjacent Si species. For samples C-200 and C-300, the naked Si-OH-Al bonds without NH_3 perturbation are less than 50% after contacting the NH_3-SCR feed gas, and hence the aggregation probability of adjacent naked Si-OH-Al is low, which limits the formation of Si-islands. For samples C-350 and C-400, with the decreased coverage of the NH_3 and increased Si-OH-Al exposure, the aggregation probability increases, and thus the formation of Si-islands becomes serious. The above results suggests that the existence of surface NH_3 adspecies could help inhibit the transformation of $Si(OAl)_4$ species and improve the hydro-stability of the BAS.

3.4.4. The location and the amount of isolated Cu^{2+} ions

EPR was used to identify the amount and coordination environment of isolated cupric ions (active sites) over CuSAPO-34. The spectra are presented in Fig. 9. All samples display similar EPR signals ($g_{//}$ = 2.36, $A_{//}$ = 133 G), which can be ascribed to the cupric ions near the face center of six-membered rings [26]. The quantitative results based on the EPR spectra are displayed in Fig. 10. For the fresh sample C, about 86% of the total Cu can be found to exist as isolated cupric ions. The amount of isolated cupric ions shows an increase for the treated catalysts C-200, C-300 and C-350. This may be ascribed to the introduction of the NH_3 during the treatment process, which facilitates the transformation of CuO to cupric ions [27]. For C-400 and C-U with trivial protection from the residual NH_3 species, the amount of cupric ions decreases by 13% and 11%, respectively. This confirms the important protective effect of the residual NH_3 adspecies upon the preservation of cupric ions.

3.4.5. The reducibility of isolated cupric ions

Previous studies by other research groups as well as our group

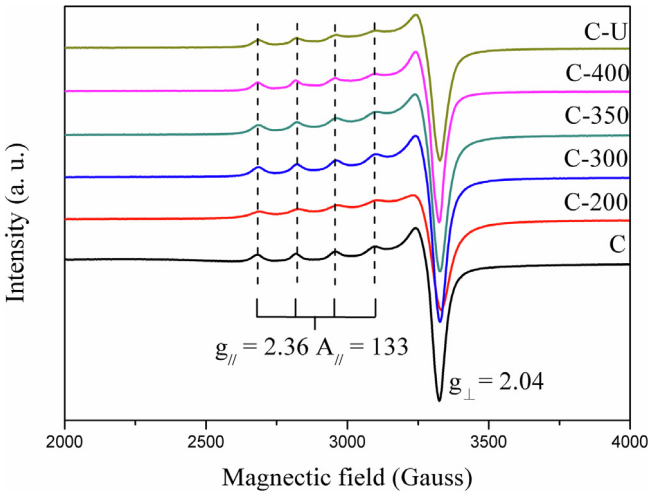

Fig. 9. EPR spectra of the CuSAPO-34 catalysts.

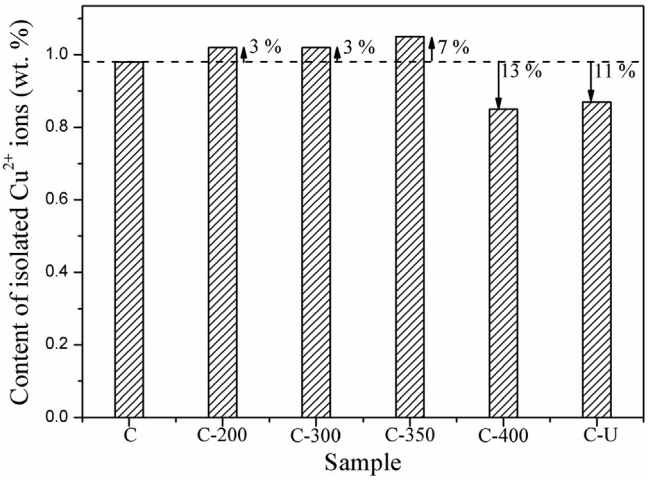

Fig. 10. The content of isolated Cu^{2+} ions over the CuSAPO-34 catalysts.

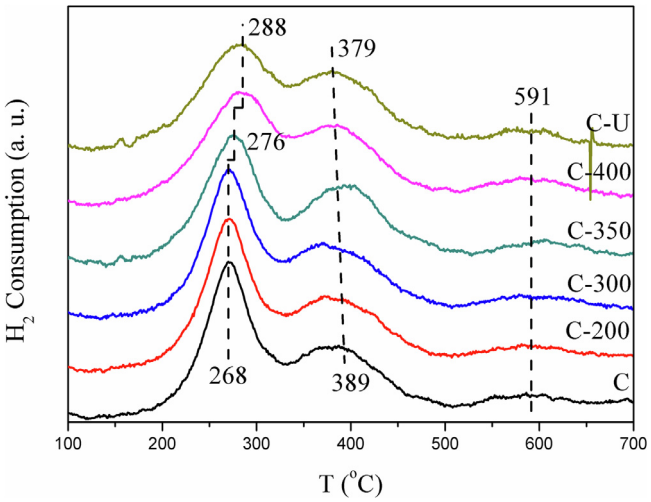

Fig. 11. H_2-TPR curves of the CuSAPO-34.

revealed that the decay of reducibility of $Cu^{2+} \rightarrow Cu^{+}$ ions over CuSAPO-34 would result in the decline of its NO_x conversion [13,28,29]. Herein, the reducibility of CuSAPO-34 was investigated by H_2-TPR. From Fig. 11, the evident peak at ca. 288 °C can be attributed to the reduction of $Cu^{2+} \rightarrow Cu^{+}$ ions; the peak around 379 °C corresponds to the further reduction of $Cu^{+} \rightarrow Cu$; the last inconspicuous peak around 591 °C may result from the reduction of isolated cuprous ions (more difficult to be reduced) [30–32].

For C-200 and C-300, compared with the fresh catalyst, similar peak shapes and positions could be observed, suggesting the comparable reducibility of Cu^{2+} ions in these treated catalysts. It is generally acknowledged that the acidities and spatial proximity between acid sites and Cu species are important to the reducibility of Cu species [13,33]. For catalysts C-200 and C-300, the well preserved acidity and Cu species status, as revealed by the aforementioned characterization results of NH_3-TPD, ^{29}Si NMR and EPR, are assumed to account for the preservation of the Cu^{2+} reducibility. However, for catalysts C-350 and C-400, the peaks corresponding to the reduction of $Cu^{2+} \rightarrow Cu^{+}$ move to higher temperature, and the reduction peak of $Cu^{+} \rightarrow Cu^{0}$ shifts to lower temperature. The decreased reducibility of $Cu^{2+} \rightarrow Cu^{+}$ ions is congruent with NH_3-SCR activity decay and should be mainly caused by the deterioration of the acid sites during the hydration treatment. The above results imply that the residual NH_3 adspecies over the catalyst after the SCR process facilitate the preservation of acid sites and the reducibility of Cu^{2+} ions against the low-temperature hydration

treatment, both of which are essential for the NH_3-SCR performance of the catalysts.

4. Conclusions

In summary, it is demonstrated that the moisture stability of CuSAPO-34 catalyst could be ameliorated by the residual adspecies after the NH_3-SCR reaction. *In-situ* DRIFTS and TPD-MS results reveal that the residual species over the catalyst surface are NH_3 adspecies, which can help inhibit the migration/aggregation of $Si(OAl)_4$ into Si islands, and thus improve the stability of the BAS. Correspondingly, the better-preserved acid sites and the existence of surface NH_3 adspecies help prevent the loss of the isolated Cu^{2+} ions and maintain their reducibility during the hydration treatment. The protective effect functions and the catalysts thus show improved low-temperature hydrostability. It is noted that this protective effect drops following the increase of NH_3-SCR reaction temperature owing to the desorption of residual NH_3 adspecies; when $T \leq 300\,^{\circ}C$, the protection effect is notable; the protection effect declines gradually and becomes weak when $T > 400\,^{\circ}C$. It is expected that our present findings could help promote the practical application of CuSAPO-34 catalyst and enhance its moisture stability by adjusting its location in the tailpipe to avoid the impact of high temperature on the NH_3 desorption over the catalyst. In addition, NH_3 pre-saturation may be applied for the freshly prepared Cu-SAPO-34 catalyst to enhance its resistance to the moisture during the storage.

Acknowledgement

We acknowledge the China Postdoctoral Science Foundation (Grant NO. 2017M621169), Key Research Program of Frontier Sciences, Chinese Academy of Sciences (Grant No. QYZDB-SSW-JSC040) and National Natural Science Foundation of China (No. 91545104, 21606221 and 21676262).

Appendix A. Supplementary data

Supplementary data to this article can be found online at https://doi.org/10.1016/j.cej.2019.05.227.

References

[1] G. Wang, R. Zhang, M.E. Gomez, L. Yang, M. Levy Zamora, M. Hu, Y. Lin, J. Peng, S. Guo, J. Meng, J. Li, C. Cheng, T. Hu, Y. Ren, Y. Wang, J. Gao, J. Cao, Z. An, W. Zhou, G. Li, J. Wang, P. Tian, W. Marrero-Ortiz, J. Secrest, Z. Du, J. Zheng, D. Shang, L. Zeng, M. Shao, W. Wang, Y. Huang, Y. Wang, Y. Zhu, Y. Li, J. Hu, B. Pan, L. Cai, Y. Cheng, Y. Ji, F. Zhang, D. Rosenfeld, P.S. Liss, R.A. Duce, C.E. Kolb, M.J. Molina, Persistent sulfate formation from London Fog to Chinese haze, Proc. Natl. Acad. Sci. (2016), https://doi.org/10.1073/pnas.1616540113.

[2] T. Johnson, Vehicular emissions in review, SAE Int. J. Engines 7 (2014) 1207–1227, https://doi.org/10.4271/2014-01-1491.

[3] A. Widd, M. Lewander, Dynamic properties of vanadium and zeolite catalysts, SAE Int. J. Fuels Lubr. 7 (2016) 911–918, https://doi.org/10.4271/2014-01-2815.

[4] S.J. Schmieg, S.H. Oh, C.H. Kim, D.B. Brown, J.H. Lee, C.H.F. Peden, D.H. Kim, Thermal durability of Cu-CHA NH3-SCR catalysts for diesel NOx reduction, Catal. Today 184 (2012) 252–261, https://doi.org/10.1016/j.cattod.2011.10.034.

[5] D.W. Fickel, E. D'Addio, J.A. Lauterbach, R.F. Lobo, The ammonia selective catalytic reduction activity of copper-exchanged small-pore zeolites, Appl. Catal. B: Environ. 102 (2011) 441–448, https://doi.org/10.1016/j.apcatb.2010.12.022.

[6] Q. Ye, L. Wang, R.T. Yang, Activity, propene poisoning resistance and hydrothermal stability of copper exchanged chabazite-like zeolite catalysts for SCR of NO with ammonia in comparison to Cu/ZSM-5, Appl. Catal. A: Gen 427–428 (2012) 24–34, https://doi.org/10.1016/j.apcata.2012.03.026.

[7] L. Ma, Y. Cheng, G. Cavataio, R.W. McCabe, L. Fu, J. Li, Characterization of commercial Cu-SSZ-13 and Cu-SAPO-34 catalysts with hydrothermal treatment for NH3-SCR of NOx in diesel exhaust, Chem. Eng. J. 225 (2013) 323–330, https://doi.org/10.1016/j.cej.2013.03.078.

[8] C. Niu, X. Shi, F. Liu, K. Liu, L. Xie, Y. You, H. He, High hydrothermal stability of Cu–SAPO-34 catalysts for the NH3-SCR of NOx, Chem. Eng. J. 294 (2016) 254–263, https://doi.org/10.1016/j.cej.2016.02.086.

[9] A. Buchholz, W. Wang, A. Arnold, M. Xu, M. Hunger, Successive steps of hydration and dehydration of silicoaluminophosphates H-SAPO-34 and H-SAPO-37 investigated by in situ CF MAS NMR spectroscopy, Microporous Mesoporous Mater. 57 (2003) 157–168, https://doi.org/10.1016/S1387-1811(02)00562-0.

[10] M. Briend, R. Vomscheid, M.J. Peltre, P.P. Man, D. Barthomeuf, Influence of the choice of the template on the short- and long-term stability of SAPO-34 zeolite, J. Phys. Chem. 99 (1995) 8270–8276, https://doi.org/10.1021/j100020a060.

[11] K. Leistner, L. Olsson, Deactivation of Cu/SAPO-34 during low-temperature NH3-SCR, Appl. Catal. B: Environ. 165 (2015) 192–199, https://doi.org/10.1016/j.apcatb.2014.09.067.

[12] J. Wang, D. Fan, T. Yu, J. Wang, T. Hao, X. Hu, M. Shen, W. Li, Improvement of low-temperature hydrothermal stability of Cu/SAPO-34 catalysts by Cu2+ species, J. Catal. 322 (2015) 84–90, https://doi.org/10.1016/j.jcat.2014.11.010.

[13] Y. Cao, D. Fan, P. Tian, L. Cao, T. Sun, S. Xu, M. Yang, Z. Liu, The influence of low-temperature hydration methods on the stability of Cu-SAPO-34 SCR catalyst, Chem. Eng. J. 354 (2018) 85–92, https://doi.org/10.1016/j.cej.2018.07.195.

[14] S.A.J. Barman, R. Khan, M. Parashar, Temperature based model approach to optimize SCR calibration for BSIV norms, SAE Tech. Paper (2016). doi: 10.4271/2016-01-1733.

[15] M.S.H. Ahari, M. Zammit, K. Price, J. Jacques, T. Pauly, L. Wang, Impact of SCR integration on N2O emissions in diesel application, SAE Int. J. Passeng. Cars – Mech. Syst., 8 (2015) 526-530. doi: 10.4271/2015-01-1034.

[16] X. Xiang, M. Yang, B. Gao, Y. Qiao, P. Tian, S. Xu, Z. Liu, Direct Cu2+ ion-exchanged into as-synthesized SAPO-34 and its catalytic application in the selective catalytic reduction of NO with NH3, RSC Adv. 6 (2016) 12544–12552, https://doi.org/10.1039/C5RA22868A.

[17] J.Y. Luo, F. Gao, K. Kamasamudram, N. Currier, C.H.F. Peden, A. Yezerets, New insights into Cu/SSZ-13 SCR catalyst acidity. Part I: Nature of acidic sites probed by NH3 titration, J. Catal. 348 (2017) 291–299, https://doi.org/10.1016/j.jcat.2017.02.025.

[18] D. Wang, Y. Jangjou, Y. Liu, M.K. Sharma, J. Luo, J. Li, K. Kamasamudram, W.S. Epling, A comparison of hydrothermal aging effects on NH3-SCR of NOx over Cu-SSZ-13 and Cu-SAPO-34 catalysts, Appl. Catal. B: Environ. 165 (2015) 438–445, https://doi.org/10.1016/j.apcatb.2014.10.020.

[19] L. Wang, W. Li, S.J. Schmieg, D. Weng, Role of Brønsted acidity in NH3 selective catalytic reduction reaction on Cu/SAPO-34 catalysts, J. Catal. 324 (2015) 98–106, https://doi.org/10.1016/j.jcat.2015.01.011.

[20] W. Su, H. Chang, Y. Peng, C. Zhang, J. Li, Reaction pathway investigation on the selective catalytic reduction of NO with NH3 over Cu/SSZ-13 at low temperatures, Environ. Sci. Technol. 49 (2015) 467–473, https://doi.org/10.1021/es503430w.

[21] D. Wang, L. Zhang, K. Kamasamudram, W.S. Epling, In Situ-DRIFTS study of selective catalytic reduction of NOx by NH3 over Cu-exchanged SAPO-34, ACS Catal. 3 (2013) 871–881, https://doi.org/10.1021/cs300843k.

[22] G.A.V. Martins, G. Berlier, S. Coluccia, H.O. Pastore, G.B. Superti, G. Gatti, L. Marchese, Revisiting the nature of the acidity in chabazite-related silicoaluminophosphates: combined FTIR and 29Si MAS NMR study, J. Phys. Chem. C 111 (2007) 330–339, https://doi.org/10.1021/jp063921q.

[23] G. Sastre, D.W. Lewis, Modelling of Bronsted acidity in AFI and CHA zeotypes, J. Chem. Soc.-Faraday Trans. 94 (1998) 3049–3058, https://doi.org/10.1039/a803843k.

[24] J. Tan, Z. Liu, X. Bao, X. Liu, X. Han, C. He, R. Zhai, Crystallization and Si incorporation mechanisms of SAPO-34, Microporous Mesoporous Mater. 53 (2002) 97–108, https://doi.org/10.1016/S1387-1811(02)00329-3.

[25] Z. Li, J. Martinez-Triguero, P. Concepcion, J. Yu, A. Corma, Methanol to olefins: activity and stability of nanosized SAPO-34 molecular sieves and control of selectivity by silicon distribution, Phys. Chem. Chem. Phys. 15 (2013) 14670–14680, https://doi.org/10.1039/C3CP52247D.

[26] A. Godiksen, F.N. Stappen, P.N.R. Vennestrøm, F. Giordanino, S.B. Rasmussen, L.F. Lundegaard, S. Mossin, Coordination environment of copper sites in Cu-CHA zeolite investigated by electron paramagnetic resonance, J. Phys. Chem. C 118 (2014) 23126–23138, https://doi.org/10.1021/jp5065616.

[27] S. Shwan, M. Skoglundh, L.F. Lundegaard, R.R. Tiruvalam, T.V.W. Janssens, A. Carlsson, P.N.R. Vennestrøm, Solid-state ion-exchange of copper into zeolites facilitated by ammonia at low temperature, ACS Catal. (2014) 16–19, https://doi.org/10.1021/cs5015139.

[28] J. Tang, M. Xu, T. Yu, H. Ma, M. Shen, J. Wang, Catalytic deactivation mechanism research over Cu/SAPO-34 catalysts for NH3-SCR (II): the impact of copper loading, Chem. Eng. Sci. 168 (2017) 414–422, https://doi.org/10.1016/j.ces.2017.04.053.

[29] D. Fan, J. Wang, T. Yu, J. Wang, X. Hu, M. Shen, Catalytic deactivation mechanism research over Cu/SAPO-34 catalysts for NH3-SCR (I): the impact of 950 °C hydrothermal aging time, Chem. Eng. Sci. 176 (2018) 285–293, https://doi.org/10.1016/j.ces.2017.10.032.

[30] J. Xue, X. Wang, G. Qi, J. Wang, M. Shen, W. Li, Characterization of copper species over Cu/SAPO-34 in selective catalytic reduction of NOx with ammonia: relationships between active Cu sites and de-NOx performance at low temperature, J. Catal. 297 (2013) 56–64, https://doi.org/10.1016/j.jcat.2012.09.020.

[31] Y. Cao, S. Zou, L. Lan, Z. Yang, H. Xu, T. Lin, M. Gong, Y. Chen, Promotional effect of Ce on Cu-SAPO-34 monolith catalyst for selective catalytic reduction of NOx with ammonia, J. Mol. Catal. A: Chem. 398 (2015) 304–311, https://doi.org/10.1016/j.molcata.2014.12.020.

[32] Y.J. Kim, J.K. Lee, K.M. Min, S.B. Hong, I.-S. Nam, B.K. Cho, Hydrothermal stability of CuSSZ13 for reducing NOx by NH3, J. Catal. 311 (2014) 447–457, https://doi.org/10.1016/j.jcat.2013.12.012.

[33] A. Martini, E. Borfecchia, K.A. Lomachenko, I.A. Pankin, C. Negri, G. Berlier, P. Beato, H. Falsig, S. Bordiga, C. Lamberti, Composition-driven Cu-speciation and reducibility in Cu-CHA zeolite catalysts: a multivariate XAS/FTIR approach to complexity, Chem. Sci. 8 (2017) 6836–6851, https://doi.org/10.1039/C7SC02266B.